ACS NANO

www.acsnano.org

ARTICLE

Core–Shell Engineered Fillers Overcome the Electrical-Thermal Conductance Trade-Off

PeiChi Liao, Haichang Guo,* Hongyu Niu, Ruijie Li, Ge Yin, Lei Kang, Liuchen Ren, Ruicong Lv, Huifeng Tian, Shizhuo Liu, Zhixin Yao, Zhenjiang Li, Yihan Wang, Lina Yang Zhang, U Sasaki, Wenxi Li, Yijie Luo, Junjie Guo, Zhi Xu, Lifen Wang, Ruqiang Zou, Shulin Bai, and Lei Liu*

Cite This: https://doi.org/10.1021/acsnano.4c09346

Read Online

ACCESS | Metrics & More | Article Recommendations | Supporting Information

ABSTRACT: The rapid development of modern electronic devices increasingly requires thermal management materials with controllable electrical properties, ranging from conductive and dielectric to insulating, to meet the needs of diverse applications. However, highly thermally conductive materials usually have a high electrical conductivity. Intrinsically highly thermally conductive, but electrically insulating materials are still limited to a few kinds of materials. To overcome the electrical-thermal conductance trade-off, here, we report a facile Pechini-based method to prepare multiple core (metal)/shell (metal oxide) engineered fillers, such as aluminum-oxide-coated and beryllium-oxide-coated Ag microspheres. In contrast to the previous *in situ* growth method which mainly focused on small-sized spheres with specific coating materials, our method combined with ultrafast joule heating treatment is more versatile and robust for varied-sized, especially large-sized core–shell fillers. Through size compounding, the as-synthesized core–shell-filled epoxy composites exhibit high isotropic thermal conductivity (~3.8 W m^{-1} K^{-1}) while maintaining high electrical resistivity (~10^{12} Ω cm) and good flowability, showing better heat dissipation properties than commercial thermally conductive packaging materials. The successful preparation of these core–shell fillers endows thermally conductive composites with controlled electrical properties for emerging electronic package applications, as demonstrated in circuit board and battery thermal management.

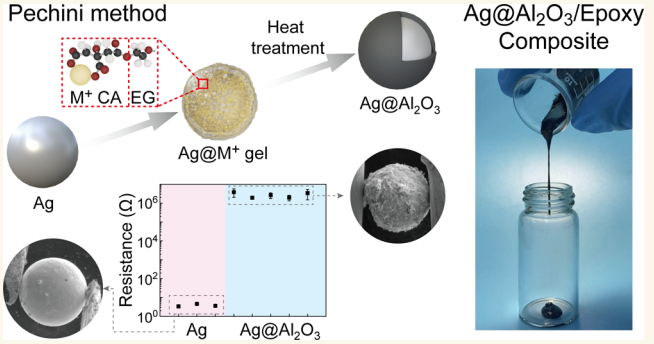

KEYWORDS: *core–shell, pechini method, thermal conductivity, electrical resistivity, thermal management*

Downloaded via SHANXI UNIV on October 25, 2024 at 07:58:42 (UTC).
See https://pubs.acs.org/sharingguidelines for options on how to legitimately share published articles.

The continued rapid development of artificial intelligence and machine learning technology has put forward increasingly higher requirements for the capabilities of integrated circuits. Nowadays, chip packaging technology is developing from classic two-dimensional (2D) packaging to 2.5-dimensional or more advanced three-dimensional (3D) packaging.[1,2] 3D stacking of multiple tiers of functional blocks can significantly enhance the capabilities of microsystems but is currently unfeasible due to inadequate thermal management, for example, the large thermal resistance across a set of device layers and their interface during the heat conduction from the hot spot to heat sink. To address this problem, recent key research mainly focuses on developing highly thermally conductive packaging materials, including epoxy-based underfill materials and thermal interface materials (TIMs) such as thermal gel, grease, pad, and thermally conductive adhesives, to minimize the thermal resistance between heterogeneous components.[3−7] In addition to high thermal conductivity (κ), it is also highly desirable for thermally conductive packaging materials to have controllable electrical properties ranging from conductive and dielectric to insulating so as to match the complex electromagnetic environment inside the device.[8−10]

Unfortunately, highly thermally conductive materials usually have high electrical conductivity, like carbon materials (*e.g.*, graphene, graphite, carbon nanotube) and metals (*e.g.*, Ag, Cu, and Au).[11−14] In commercial applications, aluminum oxide (Al_2O_3) is still the first choice for thermally conductive and insulating polymer composites, mainly due to its low cost, easy scalability, excellent thermal stability, and chemical resistance, though having relatively low κ (~30 W m^{-1} K^{-1}).[15,16] Another

Received: July 12, 2024
Revised: October 6, 2024
Accepted: October 10, 2024

© XXXX American Chemical Society

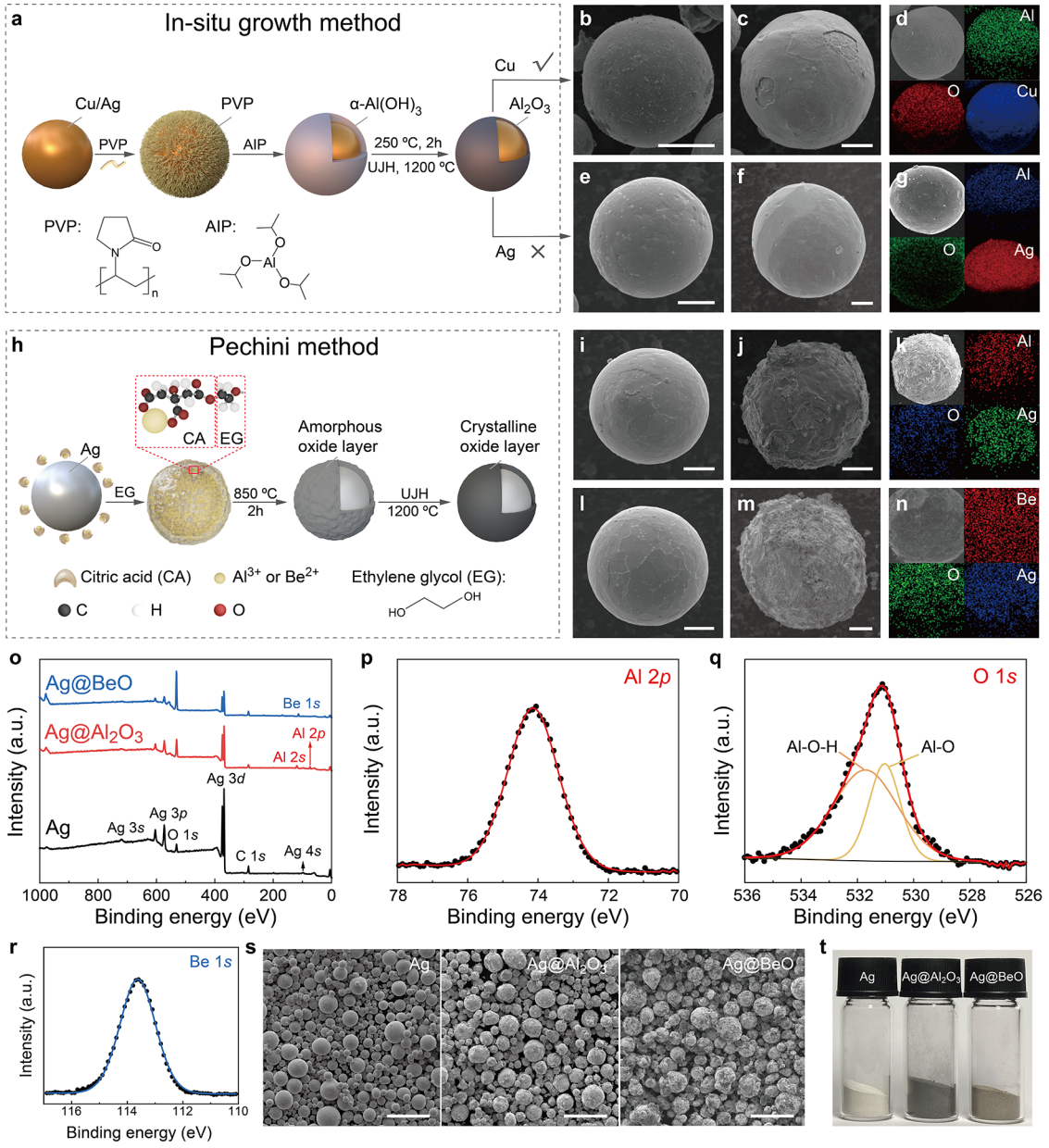

Figure 1. Synthesis and characterization of core−shell fillers. (a) Schematic of the *in situ* growth method. (b−g) SEM images and the corresponding EDS mappings showing the morphology of (b−d) Cu and (e−g) Ag spheres by the *in situ* growth method, respectively. (b, e) and (c, f) are the typical SEM images before and after the growth process, respectively. (h) Schematic of the Pechini method. (i−n) SEM images and the corresponding (k, n) EDS mappings of Ag spheres using different precursors (Al^{3+} solution for i-k and Be^{2+} solution for l-n). (i, l) and (j, m) are the typical SEM images before and after coating process, respectively. (o) XPS results of Ag, Ag@Al_2O_3, and Ag@BeO samples. (p−r) High resolution XPS spectra of (p) Al 2*p* and (q) the O 1*s* peak for Ag@Al_2O_3 and (r) the Be 1*s* peak for Ag@BeO. (s) SEM and (t) optical images of the as-synthesized Ag, Ag@Al_2O_3, and Ag@BeO spheres. Scale bar: 10 μm (b, c, e, f, i, j, l, m), 100 μm (s).

candidate is hexagonal boron nitride (*h*-BN), which has high in-plane thermal conductivity (~400 W m^{-1} K^{-1}) and excellent insulating properties (a band gap of ~6 eV).[17] The rational control of the orientation of the *h*-BN sheets can realize highly anisotropic thermal conduction along preferred direction by various assembling methods such as injection molding, doctor blading, vacuum-assisted assembly, template methods, magnetic and electric field alignment, 3D printing, and so on.[15,18−22] But usually, it cannot be used in cases where highly homogeneous thermal conduction is needed, for example, as one flowable epoxy-based underfill material. Other alternative intrinsically high-κ (>300 W m^{-1} K^{-1}) but electrically insulating materials are limited to a few materials such as diamond, aluminum nitride (AlN), silicon carbide, boron phosphide, boron arsenide, and so on.[9,23−29] But they are either expensive, of lower quality, easily hydrolyzable (AlN), or hard to scale up at this stage.

To overcome this electrical-thermal conductance trade-off, some efforts have been devoted to developing a core−shell structure by coating the metallic sphere (high-κ) with insulating layers (electrically insulating), which are summarized in Table S1.[9,30−34] However, the previous core−shell sphere-filled composites usually suffer from low thermal conductivity and unsatisfactory overall electrical-thermal-processing properties.[9] Moreover, we notice that most of these works adopted an *in situ* growth method, or in other words, directly grew the insulating layers onto the metal surfaces by using suitable surfactants and

https://doi.org/10.1021/acsnano.4c09346
ACS Nano XXXX, XXX, XXX−XXX

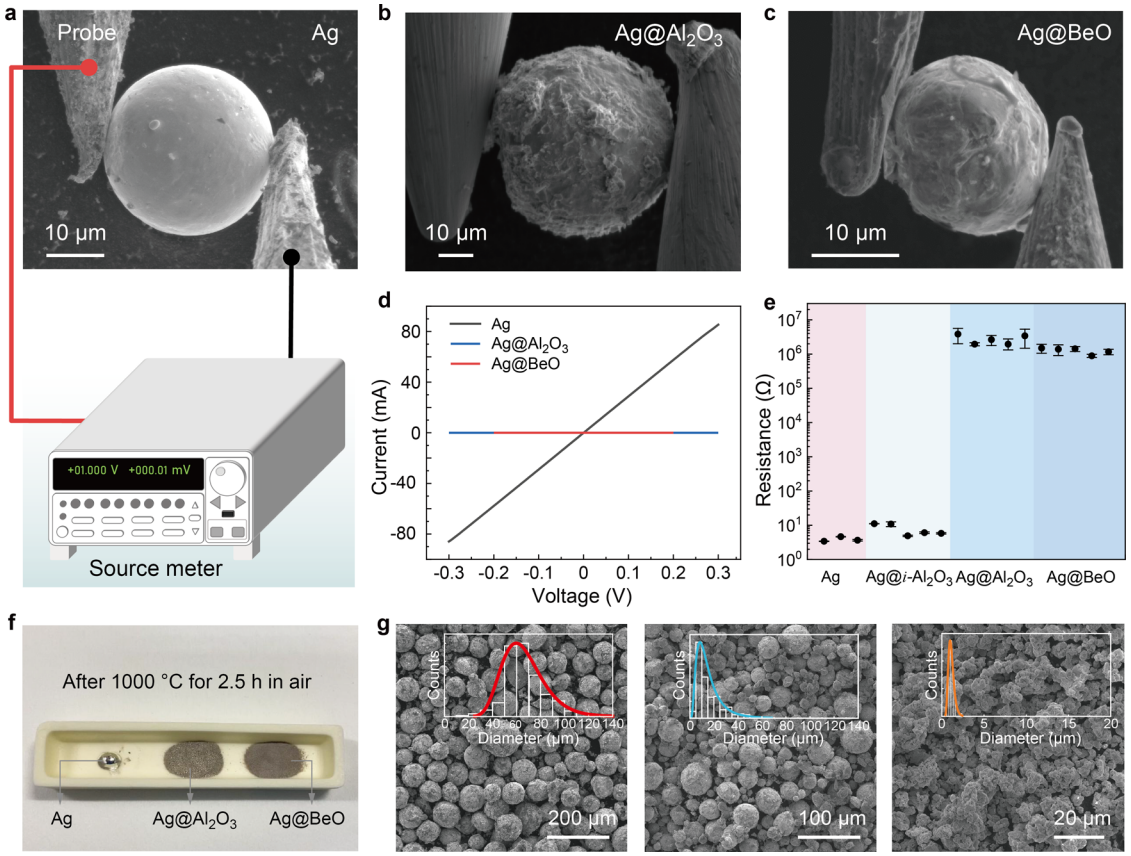

Figure 2. Evaluation of core−shell fillers at micro and macro levels. (a) Experimental setup for the resistance measurement of the single Ag sphere in the SEM chamber. (b, c) SEM images of Ag@Al_2O_3 and Ag@BeO spheres during resistance measurement, respectively. (d) Typical *I*−*V* curves for Ag, Ag@Al_2O_3, and Ag@BeO spheres. (e) The measured resistance of pristine Ag and coated Ag spheres by *in situ* growth method and Pechini method. (f) Optical images of the pristine Ag, as-synthesized Ag@Al_2O_3, and Ag@BeO powder by Pechini method after treatment by 1000 °C for 2.5 h. (g) SEM images of *l*-, *m*-, and *s*-Ag@Al_2O_3 spheres by Pechini method, respectively. Insets are the corresponding size distribution curves.

certain precursor solutions, followed by proper calcination.[35] Consequently, the resulting core−shell spheres were limited in size (several micrometers or hundreds of nanometers), which will always lead to high viscosity, low content, and low thermal conductivity of the composites.[9,32] To make the best use of the high κ of metal microspheres for thermally conductive composites, varied-sized microspheres, especially large-sized microspheres (>100 μm), are highly desired. This is because large-sized spheres can greatly decrease thermal boundary resistance, increase flowability, and form thermally conductive paths when mixing with small-sized microspheres.[36−38] Here the spherical fillers are of special preference for thermally conductive packaging applications mainly due to their isotropic thermal conductivity and easy processability. To sum up, there is still a lack of a general, effective method to coat varied-sized metal spheres, particularly large-sized spheres, with good reliability for highly thermally conductive applications.

In this work, we develop a Pechini-based method combined with an ultrafast joule heating treatment to coat high-quality Ag spheres with oxide shells such as Al_2O_3 and BeO. In contrast to the typical *in situ* growth method, the Pechini method is very versatile and robust for varied-sized core−shell fillers. We carefully confirm the robustness and insulating nature at the single-sphere level. Benefiting from the large-sized Ag@Al_2O_3 spheres and by using an optimized size compounding technique, the as-synthesized core−shell filler reinforced epoxy composites exhibit a κ of 3.8 W m^{-1} K^{-1}, higher than commercial products and most previous reports, while maintaining the high electrical resistivity and good flowability. Real device experiments verify that the core−shell fillers can be used in insulating fields such as circuit board and battery management with good reliability and improved heat dissipation performance.

RESULTS AND DISCUSSION

Wet-Chemistry Approach of Core−Shell Engineered Fillers. We started with metal microspheres, commercially available products with options of sizes and materials types, followed by oxide coating to produce core−shell filler. Although highly desired for catalytic, biomedical, electronic, and other applications, high-throughput fabrication of these hybrid spheres remains challenging.[35,39,40] The vapor deposition process (*e.g.*, physical/chemical vapor deposition) cannot wrap the inner or unexposed metal surfaces, not to mention the low deposition rate and high cost, which makes it unsuitable for large-scale manufacturing.[41] In sharp contrast, the solution process, where each core material could be isolated spatially and fully in contact with the precursor solution, is the first choice with high-cost efficiency and mass producibility. For instance, as shown in Figure 1a, the solution process called the *in situ* growth method has proven efficient in preparing Cu@*i*-Al_2O_3 spheres (see detailed fabrications in the Experimental Section). Briefly, polyvinylpyrrolidone (PVP) was first used as a surfactant to functionalize the surface of Cu spheres, which could prevent the

https://doi.org/10.1021/acsnano.4c09346
ACS Nano XXXX, XXX, XXX−XXX

incomplete formation of the shell.[31] After adding aluminum isopropoxide (AIP), a hydrolysis process of Al^{3+} was trigged which led to the formation of α-$Al(OH)_3$, followed by multiple heat treatments to convert α-$Al(OH)_3$ to crystalline Al_2O_3. The successful coating of the oxide shell layer can be easily seen from the scanning electron microscope (SEM) images in Figure 1b (bare Cu sphere) and 1c (an apparent shell with partial uncovering). Moreover, energy dispersive X-ray spectroscopy (EDS) mapping in Figure 1d indicates that the shell layer mainly consists of the elements Al and O, implying the formation of Al_2O_3 by this *in situ* growth (we label this as *i*-Al_2O_3). More SEM and X-ray photoelectron spectroscopy (XPS) characterizations of Cu@*i*-Al_2O_3 can be seen in Figure S1 and S2.

However, this *in situ* method is based on bottom-up growth on metal sphere surfaces, leading to its high sensitivity to surface functionalization. When we used the same recipe to coat Ag spheres, there was no obvious difference in sphere surfaces before and after coating (Figure 1e, f). Moreover, element distribution results (Figure 1g) show that the intensities of both Al and the O elements are weak (in sharp contrast to that of Cu@*i*-Al_2O_3 in Figure 1d), strongly suggesting the failure of Al_2O_3 coating onto Ag spheres. In other words, PVP surface functionalization does not work on the surface of Ag. Case after case denies the *in situ* approach being a general method to produce metal@metal oxide hybrids and also its opportunity to engineer constituent materials with higher thermal performance, for example, replacing Cu cores with Ag.

By borrowing the main idea from the Pechini method which is a well-established approach for commercial and in-lab synthesis of multicomponent oxides, here we introduce a Pechini-based sol−gel method to fabricate the metal@metal oxide core−shell fillers.[42−46] As shown in Figure 2h (see details in the Experimental Section), Ag powder (core material), citric acid (CA, sometimes replaced by ethylene diamine tetraacetic acid), and metal ions (Al^{3+} or Be^{2+}, or other metal cations, in principle) are mixed in the water solution to form a chelate. With the aid of ethylene glycol (EG), the chelates are cross-linked to create a gel through esterification so that Ag spheres are fully and tightly wrapped by the gel. The viscous liquid was then collected and calcined at 850 °C for 2 h to yield the amorphous metal oxide layer, followed by an ultrafast Joule heating (UJH) post-treatment (1200 °C for 2 s) to form a dense crystalline metal oxide layer.[47] Note that the Pechini method manifests as a simple and universal method by which more than 100 different mixed oxide compounds have been successfully synthesized.[48] Here we performed Al_2O_3 and BeO coating onto Ag spheres as a proof-of-concept; as shown in Figure 1j,m, the surface appears to be rough after the Pechini method when compared with those of the pristine Ag sphere (Figure 1i,l), confirming the successful coating of the Al_2O_3 and BeO layers, respectively. By cutting the Ag@Al_2O_3 sphere using a focused ion beam, a thickness of ∼5 μm for the oxide layer was confirmed (Figure S3). And a clear Ag and Al_2O_3 interface can be seen in Figure S4 using a transmission electron microscope. Furthermore, EDS results also exhibit strong intensities of Al and O signals in Figure 1k, and Be and O peaks in Figure 1n.

To further validate that the coating layers were pure Al_2O_3 or BeO rather than other contaminants, XPS characterizations were conducted. As displayed in Figure 1o, the XPS spectra show the typical peaks of pristine Ag at 368.4 eV (Ag 3*d*), 573.4 eV (Ag 3*p*), and 719.4 eV (Ag 3*s*), respectively. After coating, the Al 2*p* peak at ∼73 eV and the Al 2*s* peak at ∼119 eV arise for Ag@Al_2O_3, and the Be 1*s* peak at ∼113 eV is found in Ag@BeO. A much stronger oxygen-to-silver (O/Ag) intensity ratio than that of pristine Ag is observed for both Ag@Al_2O_3 and Ag@BeO samples. The high-resolution XPS spectra of the Al 2*p* peak (Figure 1p) located at 74.2 eV corresponds to the typical position of pure Al_2O_3.[31] The peak of O 1*s* (Figure 1q) at 531.1 eV can be deconvoluted into two peaks centered at 531.7 eV and at 531.0 eV, separately, corresponding to the hydroxyl group (Al−O−H) and the oxide ion of the Al_2O_3, respectively.[49] For Ag@BeO, Be 1*s* at 113.6 eV (Figure 1r) corresponds to the typical position of pure BeO.[50] Besides, XRD tests were also conducted and can be seen in Figure S5.

Moreover, we note that this Pechini-based method can lead to uniform coating and hundred-gram-scale preparation in the lab without sacrificing the macro powder liquidity, all of which are significant to serve as excellent thermal fillers.[42] Figure 1s displays the overall morphology of tens of pristine Ag, Ag@Al_2O_3, and Ag@BeO spheres, respectively. Every individual sphere can be clearly distinguished showing no significant aggregation, and the coating layers, although giving rise to rough morphology, can also easily be identified. On the macro scale, the colors of the Ag@Al_2O_3 and Ag@BeO powder are significantly altered when compared to pristine white Ag powder (Figure 1t). The core−shell fillers can be easily produced in bulk (*e.g.*, ∼1.5 g for each bottle) while maintaining the fluidity as good as pristine Ag powder if we tilt the vials. All these results corroborate the successful coating of the Ag spheres with metal oxide layers.

Evaluation of Core−Shell Fillers at Micro and Macro Levels. We further inspect the effect of metal oxide coating at the micro- (single-sphere) and macro levels. Basically, although there have been a lot of previous works on core−shell materials aiming for improved insulating properties, to the best of our knowledge no work has truly demonstrated the electrical insulation nature of a single sphere until now, which would be one major concern for their real applications.[9] Here, by using the SEM Nano Probe Station (Zeptools), we performed a thorough electrical test on a single sphere before and after coating in the SEM chamber. The experimental setup is schematically shown in Figure 2a, where a Ag sphere is caught by two microprobes with the aid of SEM imaging, and a source meter (Keithley 4216B) is used to record the voltage (V) and the current (I). Such a setup was also applied for Ag@Al_2O_3 and Ag@BeO spheres (Figure 2b,c). The representative measured $I-V$ curve is presented in Figure 2d. The $I-V$ curve for one pristine Ag sphere shows a linear response with a total resistance of ∼3.6 Ω (including the contact resistance), demonstrating the validity of this $I-V$ measurement. In distinct contrast, the current becomes negligible after coating with Al_2O_3 or BeO, confirming their insulating nature induced by the presence of an oxide shell.

We further carried out a series of measurements and drew a statistical conclusion. At least 10 spheres were tested for each type of sample and every single sphere was measured at least 5 times by changing the contact position between the probe and sphere. The resistance of pristine and coated Ag spheres is calculated and summarized in Figure 2e. It is worth mentioning that all of these spheres were treated by UJH, which has an important role in increasing the electrical resistivity (Figure S6). Notably, the resistance of the Ag@Al_2O_3 and Ag@BeO single sphere, although with a slight fluctuation (probably caused by the sphere size variation), is ∼6 orders of magnitude higher than that of pristine Ag spheres, confirming the insulating characteristics of these coated spheres. In spite of finite spheres being tested, we note that all of these spheres are randomly selected

https://doi.org/10.1021/acsnano.4c09346
ACS Nano XXXX, XXX, XXX−XXX

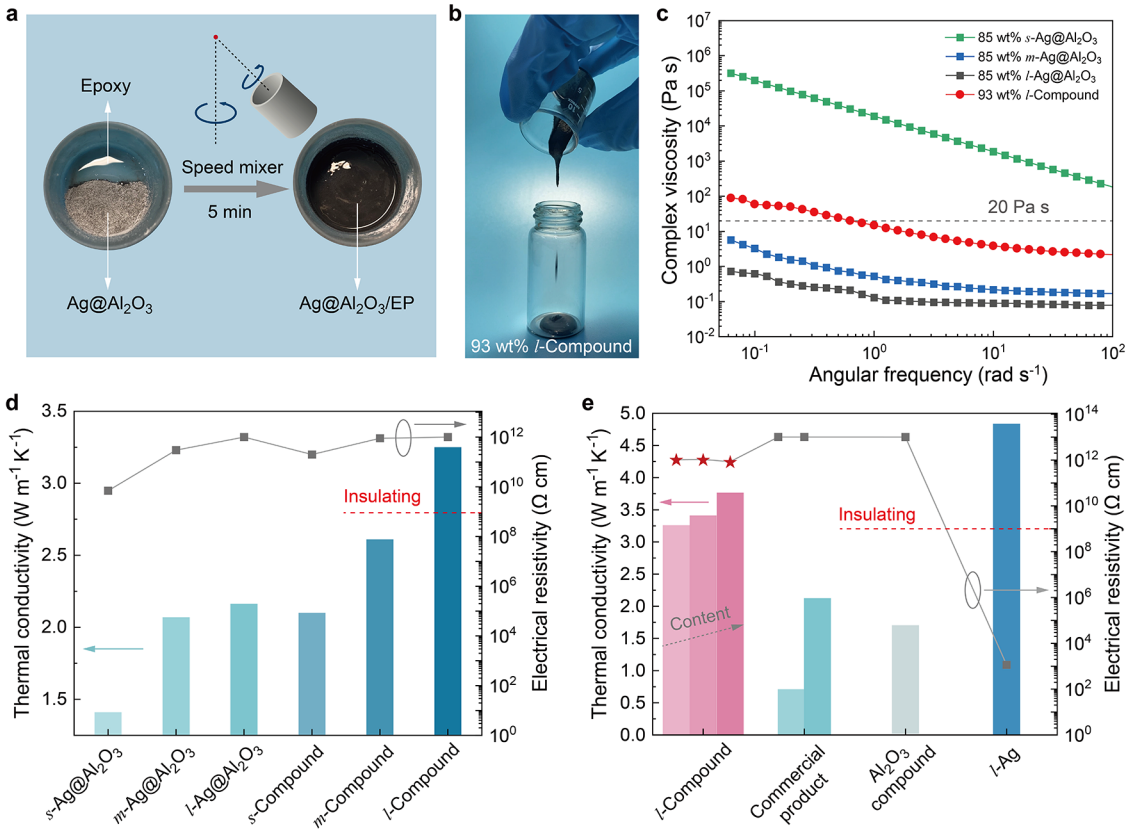

Figure 3. Properties of the core−shell sphere-filled epoxy composites used as thermally conductive packaging materials. (a) Schematic illustrating the fabrication process of $Ag@Al_2O_3$ filled epoxy composites by speed mixer. (b) Optical image showing the good fluidity of $Ag@Al_2O_3$ filled epoxy composites. (c) Viscosity of the cores-shell sphere- filled epoxy composites. (d) Thermal conductivity and electrical resistivity of different-sized $Ag@Al_2O_3$ spheres filled epoxy composites at 91.5 wt% content. (e) Comparison of the thermal conductivity and electrical resistivity of the as-synthesized $Ag@Al_2O_3$ filled epoxy composites with commercial products or typical Al_2O_3 or Ag filled epoxy composites. The content of *l*-Compound filled epoxy composites are 91.5, 93, and 94 wt% in sequence.

and all tested spheres show high resistance, strongly suggesting the full wrapping of oxide layers onto Ag spheres with sufficient oxide thicknesses. Interestingly, if we applied pressure to the $Ag@Al_2O_3$ powder using a cold-pressing machine, the single sphere could still remain insulated even under a high pressure of 0.5 MPa (Figure S7). Moreover, $Ag@i\text{-}Al_2O_3$ spheres by the *in situ* growth method were also measured, showing a comparable resistance with pristine Ag. Once again, this result verifies the failure of the Al_2O_3 coating by the *in situ* growth, which is consistent with element characterization results in Figure 1e,f. In fact, the electrical resistance of Cu and $Cu@i\text{-}Al_2O_3$ was also measured and can be seen in Figure S8. The $I-V$ measurement on a single sphere confirms the good insulating properties of the as-synthesized $Ag@Al_2O_3$ and Ag@BeO spheres at the micro level, which may address the long-standing concern of core−shell filler for real insulation applications.

To evaluate the overall encapsulation of Ag cores by metal oxide shells, high-temperature treatment of core−shell hybrids in bulk was performed. Figure 2f displays optical images of the Ag, as-synthesized $Ag@Al_2O_3$, and Ag@BeO powders by the Pechini method after 1000 °C treatment (2.5 h) in air. Note that the melting point of Ag is 962 °C so Ag powders were melted and sintered together as a ball after the high-temperature treatment. Very surprisingly, both $Ag@Al_2O_3$ and Ag@BeO powders maintained high fluidity and were free of agglomerated lumps due to silver leakage and soldering (Figure S9 and Video S1). This post-treatment, which we have not found for other previous core−shell fillers, offers a direct and unambiguous evidence that the Ag spheres are densely and robustly protected with metal oxide shells, thus preventing leakages even when Ag cores are melted. Furthermore, the Pechini method is highly universal as it can coat Ag spheres with varied sizes from 1 to 100 μm. As shown in Figure 2g, the large- (*l*-, 40−120 μm), middle- (*m*-, 10−40 μm), and small-sized (*s*-, 0.5−2 μm) $Ag@Al_2O_3$ spheres can be successfully prepared in bulk without apparent uncoated sphere.

Thermal Conductivity and Electrical Resistivity of the Epoxy Composites. The top-down Pechini-based method allows us to use intrinsically highly thermally conductive materials such as Ag as cores (Figure S10) and excellent electrically insulating metal oxides as shells, perfectly hybridizing two functions in one core−shell sphere. This advantage, together with the controlled size, the full coverage of shells, and the unaltered powder liquidity after coating, offers great benefit to utilizing these core−shell hybrids as flowable, thermally conductive but electrically insulating packaging materials such as underfill materials.[3] From one side, the large-sized core−shell fillers can effectively reduce the viscosity of the resin compared to previously reported nano- or small-sized fillers.[38] On the other side, the spherical shape ensures homogeneous and isotropic thermal conductivity, which is inaccessible by using anisotropic materials such as one-dimensional tubes/fibers and two-dimensional flakes.[51−54] Therefore, as a proof of concept, we will present our synthesized

https://doi.org/10.1021/acsnano.4c09346
ACS Nano XXXX, XXX, XXX−XXX

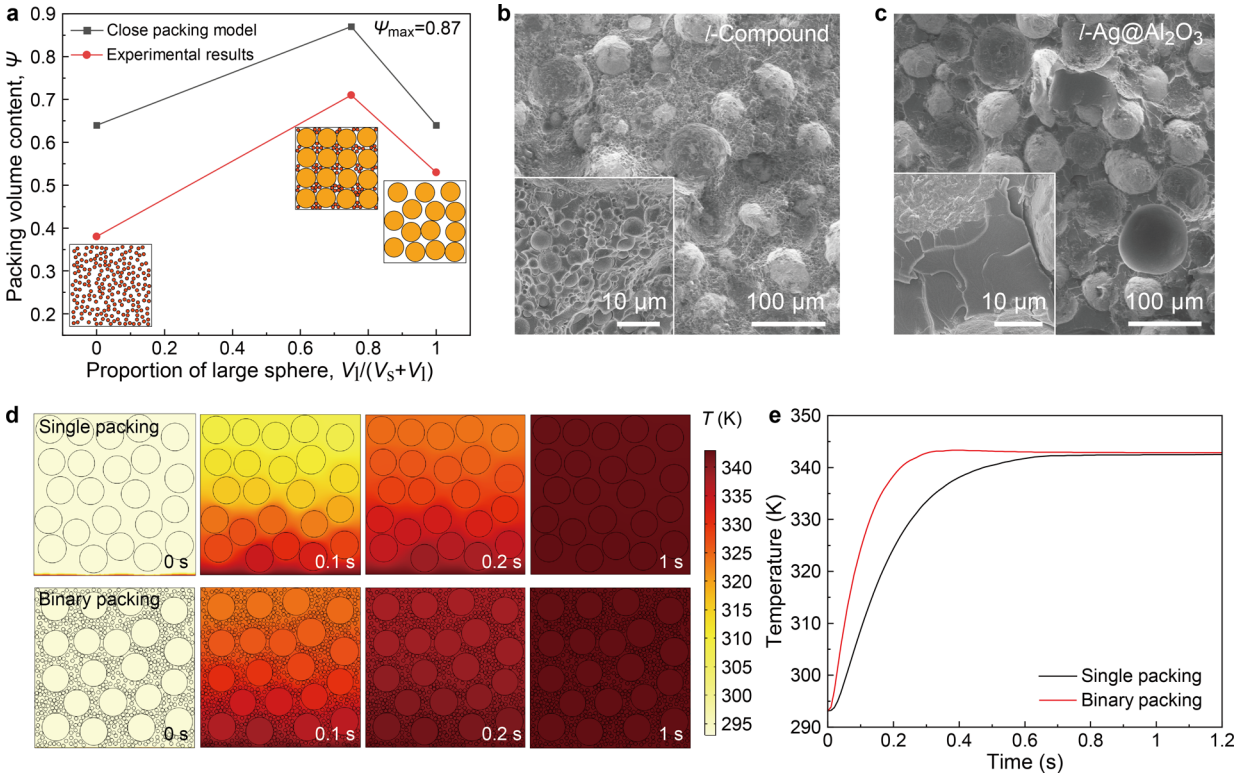

Figure 4. Effect of spherical size distribution on packing volume content and thermal conductivity for single- and binary-sphere packing systems. (a) Comparison of the maximum packing volume content between theoretical close packing model and our experimental results. (b, c) Cross-sectional SEM images of *l*-Compound and *l*-Ag@Al_2O_3 filled epoxy composites showing the sphere distribution, respectively. The insets are the corresponding zoomed-in images. (d) Simulated temperature distributions for single packing and binary packing systems with the increase of time. (e) Temperature curves for single packing and binary packing systems.

core−shell fillers for flowable, thermally conductive packaging applications in the following content.

Figure 3a shows the preparation process of core−shell filler-reinforced thermally conductive composites. In short, we directly mix Ag@Al_2O_3 powder with epoxy resin by using a speed mixer for 5 min, giving rise to visually uniform composites. The good flowability was confirmed in Figure 3b where we can easily pour the resin out from a beaker into a vial even at a high weight content of 93 wt%. To be more specific, we measured the viscosity of these epoxy composites with different filler types, including *l*-, *m*-, *s*-Ag@Al_2O_3, and *l*-Compound which was composed of *l*-Ag@Al_2O_3 and small-sized Al_2O_3 (commercial product, diameter: 1−10 μm) with a volume ratio of 3:1 (Figure 3c and S11). As expected, the *s*-Ag@Al_2O_3 filled composite has obviously higher viscosity than that of *m*-Ag@Al_2O_3 and *l*-Ag@Al_2O_3 filled composites at the same content, which should be attributed to the larger specific surface area and the irregular shape of pristine *s*-Ag (Figure S12). Intriguingly, the 93 wt% *l*-Compound filled epoxy composite still manifests a low viscosity of ~15 Pa s when the angular frequency is larger than 1 rad s^{-1}, which meets the industrial standard for underfill materials (viscosity should be below 20 Pa s).[3] Moreover, such a small value is even several orders of magnitude lower than 85 wt% *s*-Ag@Al_2O_3 filled epoxy composite, indicating the significance of size compounding in decreasing the viscosity, showing good agreement with previous work.[36]

To investigate the enhancement of thermal conductance from our core−shell fillers, we performed thorough experiments (Figures S13 and S14), and the main degree of freedom includes the filler content, the size of the microsphere, and the compounding of different-sized microspheres. Aiming for flowable thermally conductive packaging materials, one prerequisite is that the as-fabricated composite has good flowability so that the filler content used here is not that high compared to those solid thermal pad materials. We first investigate the effect of the filler size due to its important role in influencing the viscosity. As shown in Figure 3d and Table S2, when tuning the size of core−shell fillers, we find that at the same content (91.5 wt%, still flowable) the κ of *l*-Ag@Al_2O_3 filled epoxy composites (>2.0 W m^{-1} K^{-1}) is higher than that of *s*- and *m*-Ag@Al_2O_3 filled composites, which can be attributed to a higher void's content originated from the higher viscosity and poorer dispersion when using small-sized filler. Interestingly, if we replace pure Ag@Al_2O_3 spheres with a compound consisting of Ag@Al_2O_3 and Al_2O_3 with the same total weight content, *i.e.*, using the so-called size compounding technique, the κ can be significantly improved, for example, from 2.1 to 3.2 W m^{-1} K^{-1} by using *l*-Compound. This finding meets the expectation because the small-sized spheres (here, Al_2O_3) are more likely to fill the interspace between large spheres (here, *l*-Ag@Al_2O_3) and thus lead to the formation of a thermally conductive connected structure. One reason we chose commercial Al_2O_3 spheres is that they would not degrade the electrically insulating performance of the composites. Regarding the electrical properties, the core−shell filler reinforced epoxy composites reach a very high electrical resistivity of ~10^{12} Ω cm, 3 orders of magnitude higher than the insulating standard (10^9 Ω cm), indicating good insulating behavior. More importantly, even under a high pressure of 5 MPa when the composite was broken, the electrical resistivity remained almost unchanged, suggesting

https://doi.org/10.1021/acsnano.4c09346
ACS Nano XXXX, XXX, XXX−XXX

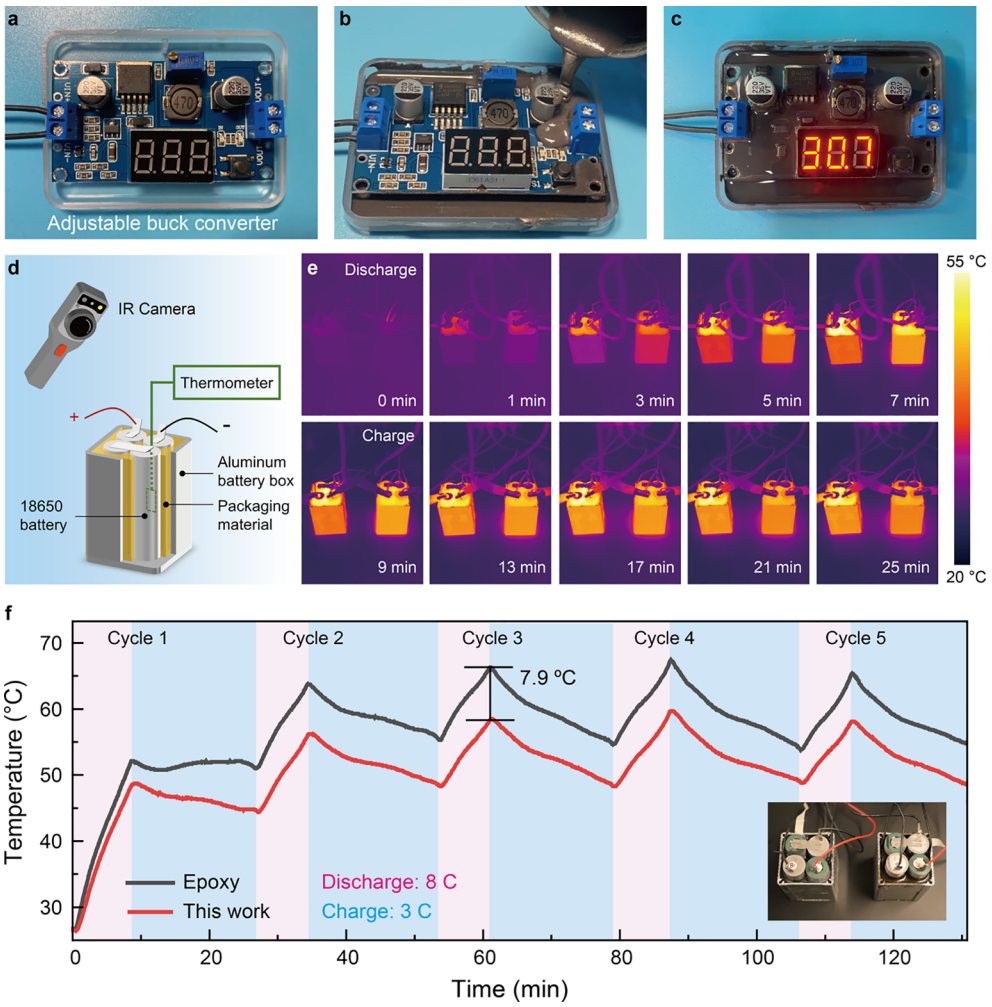

Figure 5. Device performance of the as-synthesized core−shell sphere-filled epoxy composites used as thermally conductive packaging materials. (a−c) Optical images of the adjustable buck converter (a) before, (b) during, and (c) after pouring with our synthesized Ag@Al_2O_3 filled epoxy composites, respectively. The number in (c) displays the input voltage. (d) Experimental setup for evaluating the temperature of four 18650 batteries after filling with packaging materials. (e) Temperature distribution of the testing device by IR camera during the charging and discharging process after filling with (left) pure epoxy and (right) our synthesized Ag@Al_2O_3 filled epoxy composites. (f) Temperature curves of the 18650 batteries measured by thermometer after filling with pure epoxy and our synthesized Ag@Al_2O_3 filled epoxy composites during different charging and discharging cycles. Inset: the optical image of the two testing devices.

the good stability of the core−shell fillers (Figure S15). The thermal shock and thermal cycling tests were also conducted and are shown in Figure S16.

We note that so far the highest κ of the Ag@Al_2O_3 filled epoxy composite can reach ~3.8 W m^{-1} K^{-1} at 94 wt% content with good flowability (Figure 3e), which is much larger than the commercially available products (Hasuncast RTVS21 and RTVS27−2) and pure Al_2O_3 filled epoxy composite (~1.6 W m^{-1} K^{-1}). In fact, no matter how high the claimed thermal conductivity of commercial products is, we found that the κ is less than 2 W m^{-1} K^{-1} using the same testing method, which may be due to that Al_2O_3, AlN, or other possible ceramic fillers used in their products possess a relatively lower (intrinsic) κ than that of Ag. As a controlled experiment, κ of *l*-Ag-filled epoxy composites exhibits a higher thermal conductivity of 4.8 W m^{-1} K^{-1} at a loading of 91.5 wt% but completely misses the insulating behavior (electrical resistivity: ~10^3 Ω cm). Overall, the core−shell fillers effectively overcome the electrical-thermal conductance trade-off by engineering the structure and properties at the single sphere level.

Effects of Size Compounding on Packing Volume Content and Thermal Conductivity. As discussed above, as-synthesized large core−shell spheres play an important role in reducing the viscosity and increasing thermal conductivity and electrical resistivity of the epoxy composites through rational size compounding, which is experimentally inaccessible for previously reported small core−shell fillers. To further explore the effect of size compounding, we borrowed the wisdom from a classical packing theory of spherical particles.[55,56] It is well-known that the maximum packing volume content Ψ_{max} is 0.64 if having one type of sphere (small or large, Figure 4a).[36,55,56] Notably, after compounding the small- and large-sized spheres together to form a binary packing system, Ψ_{max} can rise up to 0.87 when the proportion of large sphere is ~0.75 since small spheres can easily be embedded into the interspace between large ones to form a denser structure.[36,56] In order to ensure the good flowability of our prepared composites, the experimental maximum volume contents are naturally lower than the theoretical ones. Interestingly, after a batch of experiments, we found that the optimal volume proportion of a large sphere is 0.75 for *l*-Compound, which coincides with the theoretical

https://doi.org/10.1021/acsnano.4c09346
ACS Nano XXXX, XXX, XXX−XXX

predictions, in spite of a lower Ψ_{max} (~0.68) when compared with that in a classical model. Figure 4b,c illustrates the internal distribution states of different spheres for *l*-Compound and *l*-Ag@Al_2O_3 filled epoxy composites, respectively. It is evident that many small spheres are tightly dispersed in the interspace of large spheres for the *l*-Compound filled composite, while many "free" spaces exist in *l*-Ag@Al_2O_3 filled composites, suggesting lower packing volume content and consequently lower κ than the *l*-Compound filled composite.

In order to demonstrate thermal conductivity enhancement through size compounding, finite element calculations were performed for single-packing and binary-packing systems. The mesh generation and some basic parameters can be seen in Figure S17 and Table S3. As shown in Figure 4d, consistent with the above discussions, Ψ_{max} is only 0.53 for a single packing system (top panels) in a finite 2D space, while it is 0.69 for binary packing systems (bottom panels) due to the introduction of small-sized spheres. The bottom of the 2D model was set at a constant temperature of 343.15 K, while the left and right sides were thermally insulating and the top side was a natural convection boundary so that a unidirectional heat flow condition was generated. The binary packing system exhibits a significantly faster heat transfer rate than that in the single packing system (0.1 and 0.2 s), suggesting a higher efficient thermal conduction in the binary system. More specifically, we list the temperature profiles of the upper boundary for the two systems in Figure 4e, where a much higher temperature was observed for the binary system, indicating the higher κ. Hence based on the above analysis, we demonstrate that the size compounding technique (especially the introduction of large-sized spheres) can effectively increase the volume content and enhance the thermal conductivity, exhibiting improved performance than that of single small-sized sphere-filled polymer composites, which agrees with our experimental findings (Figure 3d).

Packaging Reliability and Heat Dissipation Performance. In order to test the reliability of our synthesized Ag@Al_2O_3-filled epoxy composites for real applications, we first tested it as an electronic packaging underfill material in an adjustable buck converter, which is used to transform a certain input voltage (*e.g.*, 12 V) to a desired output voltage (*e.g.*, 5 V). Figure 5a–c displays optical images of one converter before, during, and after pouring with our synthesized Ag@Al_2O_3 filled epoxy composites, respectively. The epoxy composites have a low viscosity so that they can penetrate and fill small gaps automatically (Figure 5b), endowing the circuit board with improved heat dissipation performance and enhanced resistance to mechanical failure. Moreover, after curing the epoxy composites at room temperature for hours, this converter still works normally at a voltage of 30.7 V (Figure 5c), demonstrating the good electrical resistivity and reliability of our synthesized Ag@Al_2O_3 filled epoxy composites.

To demonstrate the heat dissipation property of our synthesized epoxy composite, we evaluated its performance by comparing it with pure epoxy and commercial products (the same ones in Figure 3e) when they were used as packaging materials for batteries. The device setup can be seen in Figure 5d, four 18650 lithium-ion cells (2000 mAh capacity for each cell) were loaded into an aluminum battery pack with a thermometer attached to the center of one representative cell to accurately detect the temperature. The epoxy composite (or our core–shell-filled composite) was infiltrated into the gaps between the battery and the box. An infrared (IR) camera was also used to detect the spatial temperature distribution of both devices. Figure 5e illustrates the sequential temperature distribution mapping of the testing devices (left: pure epoxy; right: our-synthesized Ag@Al_2O_3 filled epoxy composite) during the charging and discharging process. It is evident that the battery encapsulated with pure epoxy has much higher temperatures than the other one encapsulated with our synthesized epoxy composite. Also, the aluminum battery pack using our synthesized composites always exhibits higher temperatures than that using pure epoxy, which is attributed to the higher κ of the synthesized composites (3.4 W m^{-1} K^{-1}) than pure epoxy (0.23 W m^{-1} K^{-1}). As shown in Figure 5f, the temperature profile suggests a stable and repeated battery temperature drop (peak value: 7.9 °C) using our epoxy composite compared to pure epoxy, implying improved heat dissipation properties. Furthermore, we also compared our synthesized composite with a commercial product, the best one we can find in the market, whose thermal conductivity has been investigated in Figure 3d. Notably, the peak temperature drop using our material can also reach 3.2 °C than the commercial product (Figure S18). We believe that the temperature drop should be enlarged when using a higher charge or discharge current. These experiments unambiguously prove the reliability and better heat dissipation performance of our Ag@Al_2O_3-filled epoxy composites.

Last but not least, the oxide coating introduced by the Pechini method is core-insensitive. In other words, it can likely be used for different materials. Using state-of-the-art measurement tools recently, low-dimensional materials, including BN nanotube, BN nanosheet, and transition metal dichalcogenides, have exhibited attractive phonon physics.[57−59] Furthermore, these inorganic nonmetal materials can be isotopically enhanced, potentially giving rise to higher *k*.[28,60,61] These materials, as the cores when coated with metal oxides by the Pechini method, are worth exploring in the future.

CONCLUSIONS

In this work, we used a facile Pechini method combined with an ultrafast joule heating treatment to coat high-quality Ag spheres (>300 W m^{-1} K^{-1}) with various insulating oxide materials like Al_2O_3 and BeO. The typical in situ growth method is usually limited to certain metal materials with several specific coating materials, and the size of the as-prepared materials is usually in several micrometers or hundreds of nanometers. In comparison, the proposed Pechini method is very versatile and robust for varied-sized core–shell fillers from 1 to 100 μm. Through size compounding, the large-sized core–shell filler can effectively decrease the viscosity and increase the thermal conductivity of the epoxy composites. The optimized thermal conductivity of the *l*-Compound filled epoxy composite can reach ~3.8 W m^{-1} K^{-1} at 94 wt% content. And the composite demonstrates good flowability while maintaining an electrical resistivity of ~10^{12} Ω cm, outperforming the available commercial products. Through such a thin shell layer coating, the Ag@Al_2O_3 materials can be reliably used in circuit board and battery management applications with improved heat dissipation properties. All these results confirm that the core–shell filler can greatly enhance the electrical resistivity of the metal materials while sustaining a high thermal conductivity, overcoming the electrical-thermal conductance trade-off of metal materials.

https://doi.org/10.1021/acsnano.4c09346
ACS Nano XXXX, XXX, XXX−XXX

EXPERIMENTAL SECTION

Materials. Commercial spherical Ag and Cu powder (purity ≥99.99%) was purchased from ZhongKe YanNuo Technical Co., Ltd. (China). Al_2O_3 microspheres were provided by the China Mineral Processing Co., Ltd. Polyvinylpyrrolidone (PVP, K30) was from Adamas-Beta, Titan Co., Ltd. (China). Aluminum nitrate nonahydrate (99.99% metal basis) was brought from Shanghai Macklin Biochemical Technology Co., Ltd. (China). Citric acid (CA, 99.5%) was provided by Energy Chemical (China). Both beryllium sulfate tetrahydrate (99.99% metal basis) and aluminum isopropoxide (AIP, ≥ 98%) were purchased from Shanghai Aladdin Biochemical Technology Co., Ltd. (China). Ethylene glycol (EG, AR) was from Concord Technology Co., Ltd. (China). Epoxy was bought from Mactac (USA).

Preparation of Cu@*i*-Al_2O_3 Sphere by the *In Situ* Growth Method. First, 2 g of PVP was dissolved in 100 mL of deionized water, and then 2 g of Cu particles were added to the solution. After stirring for 3 h, the PVP functionalized Cu particles (Cu@PVP) were obtained. Next, to prepare an $Al(OH)_3$ solution, we put 1g AIP in 150 mL ethanol and then heated it to 45 °C under thorough stirring, followed by the addition of hydrochloric acid to realize a pH value of 2−4. After continuous stirring at 45 °C for ∼1h, a stable and transparent $Al(OH)_3$ solution was finally obtained. The Cu@PVP was added into the $Al(OH)_3$ solution and reacted for ∼1 h. After gently filtering, the resulting $Al(OH)_3$ decorated powder was obtained, which was then rinsed with ethanol 3 times. With heat treatment at 250 °C for 2 h, Cu@*i*-Al_2O_3 particles were successfully synthesized.

Preparation of Ag@Al_2O_3 and Ag@BeO Sphere by Pechini Method. We first prepare the Pechini solution by dissolving aluminum nitrate hydrate or beryllium sulfate tetrahydrate in deionized water with quantitative citric acid monohydrate. The ratio of metal salts to citric acid mol is 1:3 and the concentration is 0.4 M. After that, Ag powder was added to the solution. Ethylene glycol was then slowly dropped into the solution at 120 °C with constant stirring until a homogeneous, high-viscosity gel was formed. The viscous liquid was soon transferred to an alumina crucible, put into a muffle furnace, and heated at 850 °C for 2h. The heating rate was set as 25 °C min^{-1} from room temperature to 850 °C. After naturally cooling to room temperature, the resulting aggregated gray or black powder was ground to get the final dispersed core−shell powder.

Ultrafast Joule Heating Process. First, the raw powder was placed in a crucible and then sandwiched between two thermally conductive carbon felts. After the reaction was ramped up to 1200 °C within 5 s and held for 2 s in vacuum, the dense crystalline metal oxide layer was formed.

Preparation of Core−Shell Filler Reinforced Epoxy Composites. The core−shell filler-filled epoxy composites are directly prepared by a speed mixer. Specifically, core−shell powder and epoxy (viscosity: ∼600 cP) with a certain weight ratio were mixed at 500 rpm for 2 min and 1200 rpm for 3 min. The resulting homogeneous liquid was cured at room temperature for 24 h or 90 °C for 1 h to obtain the final epoxy composites.

Characterizations. The microscopic morphologies were observed by a field emission scanning electron microscope (TESCAN VEGA 3 LMH). The diameter of each sphere was calculated automatically using the plug-in that comes with SEM. Thermogravimetric analysis (TGA) was obtained by an SDT Q600 (TA). The thermal diffusivities of films were measured by a laser flash analyzer (LFA 467, NETZSCH, Germany). The specific heat capacities of the films were measured by differential scanning calorimetry (Q100, TA, USA). The ultrafast Joule heating process was performed by ZKJY-HTS (Shenzhen Zhongke Jingyan Technology Co. Ltd.). The electrical measurements on single sphere fillers were performed with an SEM Nano Probe Station (Zeptools).

ASSOCIATED CONTENT

Supporting Information

The Supporting Information is available free of charge at https://pubs.acs.org/doi/10.1021/acsnano.4c09346.

Comparison of the properties of previous core-shell sphere-filled composites with this work; Detailed parameters for calculating the thermal conductivity of epoxy composites; Basic parameters for finite element simulations; Optical, SEM, XPS, XRD and electrical characterizations of Cu and Cu@*i*-Al_2O_3 spheres; identification of the oxide layer thickness of Ag@Al_2O_3 sphere; TEM and EDS characterizations at Ag and Al_2O_3 interface; effects of UJH treatment; electrical conductance of Ag@Al_2O_3 under different mechanical pressure; SEM images core−shell spheres after 1000 °C treatment for 2.5 h; optical image of bulk Ag for thermal conductivity measurement; viscosity of the core−shell sphere-filled epoxy composites with the increase of the content; SEM image of *s*-Ag powder; controlled experiments to explore the effects of content, coating materials, and size compounding on the thermal conductivity of the epoxy composites; optical image of the core−shell sphere-filled epoxy composites for thermal conductivity measurements; electrical resistivity of *l*-Compound filled epoxy composite under different mechanical pressures; thermal reliability test for Ag@Al_2O_3 spheres and the as-prepared composites; mesh generation for COMSOL simulations; temperature curves of the 18650 battery for our epoxy composites and commercial products and demonstration of the good fluidity of the core−shell powder after 1000 °C treatment for 2.5 h (PDF)

Demonstration of the excellent fluidity of the core-shell powder after 1000 °C treatment for 2.5 h (MP4)

AUTHOR INFORMATION

Corresponding Authors

Haichang Guo − *School of Materials Science and Engineering, Peking University, Beijing 100871, China*; Email: haichang@pku.edu.cn

Lei Liu − *School of Materials Science and Engineering, Peking University, Beijing 100871, China*; orcid.org/0000-0002-7226-8423; Email: l_liu@pku.edu.cn

Authors

PeiChi Liao − *School of Materials Science and Engineering, Peking University, Beijing 100871, China*

Hongyu Niu − *School of Materials Science and Engineering, Peking University, Beijing 100871, China*

Ruijie Li − *School of Materials Science and Engineering, Peking University, Beijing 100871, China*

Ge Yin − *School of Materials Science and Engineering, Peking University, Beijing 100871, China*

Lei Kang − *School of Materials Science and Engineering, Peking University, Beijing 100871, China*

Liuchen Ren − *School of Materials Science and Engineering, Peking University, Beijing 100871, China*

Ruicong Lv − *School of Materials Science and Engineering, Peking University, Beijing 100871, China*

Huifeng Tian − *School of Materials Science and Engineering, Peking University, Beijing 100871, China*

Shizhuo Liu − *School of Materials Science and Engineering, Peking University, Beijing 100871, China*

Zhixin Yao − *Key Laboratory of Interface Science and Engineering in Advanced Materials, Ministry of Education, Taiyuan University of Technology, Taiyuan 030024, China*

Zhenjiang Li − *School of Materials Science and Engineering, Peking University, Beijing 100871, China*

https://doi.org/10.1021/acsnano.4c09346
ACS Nano XXXX, XXX, XXX−XXX

Yihan Wang − *School of Materials Science and Engineering, Peking University, Beijing 100871, China*
Lina Yang Zhang − *School of Materials Science and Engineering, Peking University, Beijing 100871, China*
U Sasaki − *School of Materials Science and Engineering, Peking University, Beijing 100871, China*
Wenxi Li − *School of Materials Science and Engineering, Peking University, Beijing 100871, China*
Yijie Luo − *School of Materials Science and Engineering, Peking University, Beijing 100871, China*
Junjie Guo − *Key Laboratory of Interface Science and Engineering in Advanced Materials, Ministry of Education, Taiyuan University of Technology, Taiyuan 030024, China;* orcid.org/0000-0002-3414-3734
Zhi Xu − *Songshan Lake Materials Laboratory, Dongguan, Guangdong 523808, China*
Lifen Wang − *China Beijing National Laboratory for Condensed Matter Physics, Institute of Physics, Chinese Academy of Sciences, Beijing 100190, China;* orcid.org/0000-0002-8468-5048
Ruqiang Zou − *School of Materials Science and Engineering, Peking University, Beijing 100871, China;* orcid.org/0000-0003-0456-4615
Shulin Bai − *School of Materials Science and Engineering, Peking University, Beijing 100871, China;* orcid.org/0000-0001-9177-7525

Complete contact information is available at: https://pubs.acs.org/10.1021/acsnano.4c09346

Author Contributions

L.L. and H.G. conceived and supervised the project. P.L. and H.G. contributed equally to this work. H.N. developed the COMSOL simulations. P.L., R.L., G.Y., L.K., L.R., and R.L. carried out the sample preparations. P.L., H.T., S.L., Z.Y., Z.L., Y.W., L.Y.Z., and S.U. performed the general characterizations. W. L., Y. L., and R.Z. performed the FIB and TEM characterizations. J.G. and Z.X. performed the SEM-probe measurements. L.W. and S.B. performed the thermal conductance measurements. All authors discussed the results. H.G. and L.L. wrote the manuscript with the inputs from all authors.

Notes

The authors declare no competing financial interest.

ACKNOWLEDGMENTS

This work was supported by the National Key R&D Program of China (2019YFA0307800, 2021YFA1400500), the Beijing Natural Science Foundation (JQ23004), the National Natural Science Foundation of China (52322311), and the China Postdoctoral Science Foundation (BX20230002). L.W. is grateful for the support from the Youth Innovation Promotion Association of CAS (2020009). L.L. acknowledges the support of facilities from Peking Nanofab. We thank the Materials Processing and Analysis Center, Peking University for assistance with XRD, XPS, SEM, TEM, and EDS characterizations.

REFERENCES

(1) Takahashi, K.; Umemoto, M.; Tanaka, N.; Tanida, K.; Nemoto, Y.; Tomita, Y.; Tago, M.; Bonkohara, M. Ultra-High-Density Interconnection Technology of Three-Dimensional Packaging. *Microelectron. Reliab.* **2003**, *43*, 1267−1279.
(2) Liu, D.; Park, S. Three-Dimensional and 2.5 Dimensional Interconnection Technology: State of the Art. *J. Electron. Packag.* **2014**, *136*, No. 014001.
(3) Wen, Y.; Chen, C.; Ye, Y.; Xue, Z.; Liu, H.; Zhou, X.; Zhang, Y.; Li, D.; Xie, X.; Mai, Y. W. Advances on Thermally Conductive Epoxy-Based Composites as Electronic Packaging Underfill Materials—A Review. *Adv. Mater.* **2022**, *34*, No. 2201023.
(4) Sun, Z.; Li, J.; Yu, M.; Kathaperumal, M.; Wong, C.-P. A Review of the Thermal Conductivity of Silver-Epoxy Nanocomposites As Encapsulation Material for Packaging Applications. *Chem. Eng. J.* **2022**, *446*, No. 137319.
(5) Prasher, R. Thermal Interface Materials: Historical Perspective, Status, and Future Directions. *Proc. IEEE* **2006**, *94*, 1571−1586.
(6) Dai, W.; Ma, T.; Yan, Q.; Gao, J.; Tan, X.; Lv, L.; Hou, H.; Wei, Q.; Yu, J.; Wu, J.; Yao, Y.; Du, S.; Sun, R.; Jiang, N.; Wang, Y.; Kong, J.; Wong, C.; Maruyama, S.; Lin, C. T. Metal-Level Thermally Conductive yet Soft Graphene Thermal Interface Materials. *ACS Nano* **2019**, *13*, 11561−11571.
(7) Niu, H.; Guo, H.; Kang, L.; Ren, L.; Lv, R.; Bai, S. Vertical Alignment of Anisotropic Fillers Assisted by Expansion Flow in Polymer Composites. *Nano-Micro Lett.* **2022**, *14*, 153.
(8) Li, R.; Yang, X.; Li, J.; Shen, Y.; Zhang, L.; Lu, R.; Wang, C.; Zheng, X.; Chen, H.; Zhang, T. Review on Polymer Composites with High Thermal Conductivity and Low Dielectric Properties for Electronic Packaging. *Mater. Today phys.* **2022**, *22*, No. 100594.
(9) Chen, Q.; Yang, K.; Feng, Y.; Liang, L.; Chi, M.; Zhang, Z.; Chen, X. Recent Advances in Thermal-Conductive Insulating Polymer Composites with Various Fillers. *Compos. Part A-Appl. S.* **2024**, *178*, No. 107998.
(10) Niu, H.; Ren, Y.; Guo, H.; Małycha, K.; Orzechowski, K.; Bai, S.-L. Recent Progress on Thermally Conductive and Electrical Insulating Rubber Composites: Design. *Processing and Applications. Compos. Commun.* **2020**, *22*, No. 100430.
(11) Chen, L.; Liu, T. H.; Wang, X.; Wang, Y.; Cui, X.; Yan, Q.; Lv, L.; Ying, J.; Gao, J.; Han, M.; Yu, J.; Song, C.; Gao, J.; Sun, R.; Xue, C.; Jiang, N.; Deng, T.; Nishimura, K.; Yang, R.; Lin, C. T.; Dai, W. Near-Theoretical Thermal Conductivity Silver Nanoflakes as Reinforcements in Gap-Filling Adhesives. *Adv. Mater.* **2023**, *35*, No. 2211100.
(12) Balandin, A. A. Thermal Properties of Graphene and Nanostructured Carbon Materials. *Nat. Mater.* **2011**, *10*, 569−581.
(13) Suh, D.; Moon, C. M.; Kim, D.; Baik, S. Ultrahigh Thermal Conductivity of Interface Materials by Silver-Functionalized Carbon Nanotube Phonon Conduits. *Adv. Mater.* **2016**, *28*, 7220−7227.
(14) Abdul Jaleel, S. A.; Kim, T.; Baik, S. Covalently Functionalized Leakage-Free Healable Phase-Change Interface Materials with Extraordinary High-Thermal Conductivity and Low-Thermal Resistance. *Adv. Mater.* **2023**, *35*, No. 2300956.
(15) Hong, H.; Kim, J.; Kim, T.-I. Effective Assembly of Nano-Ceramic Materials for High and Anisotropic Thermal Conductivity in a Polymer Composite. *Polymers* **2017**, *9*, 413.
(16) Ouyang, Y.; Bai, L.; Tian, H.; Li, X.; Yuan, F. Recent Progress of Thermal Conductive Ploymer Composites: Al_2O_3 Fillers, Properties and Applications. *Compos. Part A-Appl. S.* **2022**, *152*, No. 106685.
(17) Cai, Q.; Li, L. H.; Mateti, S.; Bhattacharjee, A.; Fan, Y.; Huang, S.; Chen, Y. I. Boron Nitride Nanosheets: Thickness-Related Properties and Applications. *Adv. Funct. Mater.* **2024**, *34*, 2205120.
(18) Hong, H.; Jung, Y. H.; Lee, J. S.; Jeong, C.; Kim, J. U.; Lee, S.; Ryu, H.; Kim, H.; Ma, Z.; Kim, T. i. Anisotropic Thermal Conductive Composite by the Guided Assembly of Boron Nitride Nanosheets for Flexible and Stretchable Electronics. *Adv. Funct. Mater.* **2019**, *29*, No. 1902575.
(19) Kang, S. J.; Hong, H.; Jeong, C.; Lee, J. S.; Ryu, H.; Yang, J.-H.; Kim, J. U.; Shin, Y. J.; Kim, T.-I. Avoiding Heating Interference and Guided Thermal Conduction in Stretchable Devices Using Thermal Conductive Composite Islands. *Nano Res.* **2021**, *14*, 3253−3259.
(20) He, H.; Peng, W.; Liu, J.; Chan, X. Y.; Liu, S.; Lu, L.; Le Ferrand, H. Microstructured BN Composites with Internally Designed High Thermal Conductivity Paths for 3D Electronic Packaging. *Adv. Mater.* **2022**, *34*, No. 2205120.
(21) Guo, H.; Niu, H.; Zhao, H.; Kang, L.; Ren, Y.; Lv, R.; Ren, L.; Maqbool, M.; Bashir, A.; Bai, S. Highly Anisotropic Thermal Conductivity of Three-Dimensional Printed Boron Nitride-Filled

Thermoplastic Polyurethane Composites: Effects of Size, Orientation, Viscosity, and Voids. *ACS Appl. Mater. Interfaces* **2022**, *14*, 14568−14578.
(22) Niu, H.; Guo, H.; Kang, L.; Ren, L.; Lv, R.; Liu, L.; Bashir, A.; Bai, S. Highly Thermally Conductive and Soft Thermal Interface Materials Based on Vertically Oriented Boron Nitride Film. *Compos. Part B-Eng.* **2024**, *272*, No. 111219.
(23) Tian, F.; Song, B.; Chen, X.; Ravichandran, N. K.; Lv, Y.; Chen, K.; Sullivan, S.; Kim, J.; Zhou, Y.; Liu, T.-H.; Goni, M.; Ding, Z.; Sun, J.; Gamage, G. A. G. U.; Sun, H.; Ziyaee, H.; Huyan, S.; Deng, L.; Zhou, J.; Schmidt, A. J.; Chen, S.; Chu, C.-W.; Huang, P. Y.; Broido, D.; Shi, L.; Chen, G.; Ren, Z. Unusual High Thermal Conductivity in Boron Arsenide Bulk Crystals. *Science* **2018**, *361*, 582−585.
(24) Li, S.; Zheng, Q.; Lv, Y.; Liu, X.; Wang, X.; Huang, P. Y.; Cahill, D. G.; Lv, B. High Thermal Conductivity in Cubic Boron Arsenide Crystals. *Science* **2018**, *361*, 579−581.
(25) Kang, J. S.; Li, M.; Wu, H.; Nguyen, H.; Hu, Y. Experimental Observation of High Thermal Conductivity in Boron Arsenide. *Science* **2018**, *361*, 575−578.
(26) Cheng, Z.; Liang, J.; Kawamura, K.; Zhou, H.; Asamura, H.; Uratani, H.; Tiwari, J.; Graham, S.; Ohno, Y.; Nagai, Y.; Feng, T.; Shigekawa, N.; Cahill, D. G. High Thermal Conductivity in Wafer-Scale Cubic Silicon Carbide Crystals. *Nat. Commun.* **2022**, *13*, 7201.
(27) Guerra, V.; Wan, C.; McNally, T. Thermal Conductivity of 2D Nano-Structured Boron Nitride (BN) and Its Composites with Polymers. *Prog. Mater. Sci.* **2019**, *100*, 170−186.
(28) Li, Y.; Wen, X.; Tan, C.; Li, N.; Li, R.; Huang, X.; Tian, H.; Yao, Z.; Liao, P.; Yu, S.; Liu, S.; Li, Z.; Guo, J.; Huang, Y.; Gao, P.; Wang, L.; Bai, S.; Liu, L. Synthesis of Centimeter-Scale High-Quality Polycrystalline Hexagonal Boron Nitride Films from Fe Fluxes. *Nanoscale* **2021**, *13*, 11223−11231.
(29) Yu, S.; Liao, P.; Zhang, Y.; Li, Y.; Tian, H.; Li, R.; Liu, S.; Yao, Z.; Li, Z.; Wang, Y.; Zhang, L. Y.; U, S.; Guo, J.; Wang, L.; Bai, S.; Chen, J.; Bai, X.; Liu, L. Hydrogen-Bond-Mediated Surface Functionalization of Boron Nitride Micro-Lamellae toward High Thermal Conductive Papers. *Adv. Mater. Interfaces* **2023**, *10*, No. 2202196.
(30) Zhou, Y.; Wang, L.; Zhang, H.; Bai, Y.; Niu, Y.; Wang, H. Enhanced High Thermal Conductivity and Low Permittivity of Polyimide Based Composites by Core-Shell Ag@SiO_2 Nanoparticle Fillers. *Appl. Phys. Lett.* **2012**, *101*, No. 012903.
(31) Wang, Z.; Zhang, Y.; Yi, J.; Cai, N.; Guo, J. Core-Shell Cu@Al_2O_3 Fillers for Enhancing Thermal Conductivity and Retaining Electrical Insulation of Epoxy Composites. *J. Alloys Compd.* **2022**, *928*, No. 167123.
(32) Li, J.; Li, X.; Zheng, Y.; Liu, Z.; Tian, Q.; Liu, X. New Underfill Material Based on Copper Nanoparticles Coated with Silica for High Thermally Conductive and Electrically Insulating Epoxy Composites. *J. Mater. Sci.* **2019**, *54*, 6258−6271.
(33) Mao, D.; Chen, J.; Ren, L.; Zhang, K.; Yuen, M. M. F.; Zeng, X.; Sun, R.; Xu, J.-B.; Wong, C.-P. Spherical Core-Shell Al@Al_2O_3 Filled Epoxy Resin Composites As High-Performance Thermal Interface Materials. *Compos. Part A-Appl. S.* **2019**, *123*, 260−269.
(34) Jiang, Y.; Li, M.; Chen, C.; Xue, Z.; Xie, X.; Zhou, X.; Mai, Y.-W. Effect of Elastic Modulus Mismatch of Epoxy/Titanium Dioxide Coated Silver Nanowire Composites on the Performance of Thermal Conductivity. *Compos. Sci. Technol.* **2018**, *165*, 206−213.
(35) Chaudhuri, R. G.; Paria, S. Core/Shell Nanoparticles: Classes, Properties, Synthesis Mechanisms, Characterization, and Applications. *Chem. Rev.* **2012**, *112*, 2373−2433.
(36) Chen, C.; Xue, Y.; Li, X.; Wen, Y.; Liu, J.; Xue, Z.; Shi, D.; Zhou, X.; Xie, X.; Mai, Y.-W. High-Performance Epoxy/Binary Spherical Alumina Composite As Underfill Material for Electronic Packaging. *Compos. Part A-Appl. S.* **2019**, *118*, 67−74.
(37) Zhong, A.; Xie, C.; Gou, B.; Zhou, J.; Xu, H.; Yu, S.; Zhang, D.; Bi, C.; Cai, H.; Li, L.; Wang, R. Recyclable Technology of Thermosetting Resins for High Thermal Conductivity Materials Based on Physical Crushing. *Energy Environ. Mater.* **2024**, *7*, No. e12762.
(38) Wang, Y.; Liu, T.; Zhang, H.; Luo, N.; Chen, F.; Fu, Q. Effect of Spherical Alumina Crystalline Phase Content and Particle Size Distribution Polydispersity on the Properties of Silicone Rubber Composites. *Compos. Sci. Technol.* **2023**, *243*, No. 110273.
(39) Chatterjee, K.; Sarkar, S.; Rao, K. J.; Paria, S. Core/Shell Nanoparticles in Biomedical Applications. *Adv. Colloid Interface Sci.* **2014**, *209*, 8−39.
(40) Galogahi, F. M.; Zhu, Y.; An, H.; Nguyen, N.-T. Core-Shell Microparticles: Generation Approaches and Applications. *J. Sci-Adv. Mater. Dev.* **2020**, *5*, 417−435.
(41) Wadley, H. N. G.; Zhou, A. X.; Johnson, R. A.; Neurock, M. Mechanisms, Models and Methods of Vapor Deposition. *Prog. Mater. Sci.* **2001**, *46*, 329−377.
(42) Dimesso, L. Pechini Processes: An Alternate Approach of the Sol-Gel Method, Preparation, Properties, and Applications. In *Handbook of Sol-Gel Science and Technology: Processing, Characterization and Applications*, Klein, L.; Aparicio, M.; Jitianu, A., Eds.; Springer International Publishing: Cham, 2018; pp. 1067−1088.
(43) Liu, W.; Farrington, G.; Chaput, F.; Dunn, B. Synthesis and Electrochemical Studies of Spinel Phase $LiMn_2O_4$ Cathode Materials Prepared by the Pechini Process. *J. Electrochem. Soc.* **1996**, *143*, 879.
(44) Agarwal, V.; Liu, M. L. Preparation of Barium Cerate-Based Thin Films Using a Modified Pechini Process. *J. Mater. Sci.* **1997**, *32*, 619−625.
(45) Hossain, M. S.; Bhuiyan, A. H.; Nakane, K. Thermal Conductivity of Polyurethane Sheets Containing Beryllium Oxide Nanofibers. *RSC Adv.* **2022**, *12*, 30125−30134.
(46) Zaki, T.; Kabel, K. I.; Hassan, H. Preparation of High Pure α-Al_2O_3 Nanoparticles at Low Temperatures Using Pechini Method. *Ceram. Int.* **2012**, *38*, 2021−2026.
(47) Wang, C.; Ping, W.; Bai, Q.; Cui, H.; Hensleigh, R.; Wang, R.; Brozena, A. H.; Xu, Z.; Dai, J.; Pei, Y.; Zheng, C.; Pastel, G.; Gao, J.; Wang, X.; Wang, H.; Zhao, J.-C.; Yang, B.; Zheng, X.; Luo, J.; Mo, Y.; Dunn, B.; Hu, L. A General Method to Synthesize and Sinter Bulk Ceramics in Seconds. *Science* **2020**, *368*, 521−526.
(48) Kim, H. J.; Kearney, K. L.; Le, L. H.; Pekarek, R. T.; Rose, M. J. Platinum-Enhanced Electron Transfer and Surface Passivation through Ultrathin Film Aluminum Oxide (Al_2O_3) on Si (111)-CH_3 Photoelectrodes. *ACS Appl. Mater. Interfaces* **2015**, *7*, 8572−8584.
(49) Mallinson, C. F.; Castle, J. E. Beryllium and Beryllium Oxide by XPS. *Surf. Sci. Spectra* **2013**, *20*, 86−96.
(50) Guo, H.; Zhao, H.; Niu, H.; Ren, Y.; Fang, H.; Fang, X.; Lv, R.; Maqbool, M.; Bai, S. Highly Thermally Conductive 3D Printed Graphene Filled Polymer Composites for Scalable Thermal Management Applications. *ACS Nano* **2021**, *15*, 6917−6928.
(51) Uetani, K.; Ata, S.; Tomonoh, S.; Yamada, T.; Yumura, M.; Hata, K. Elastomeric Thermal Interface Materials with High Through-Plane Thermal Conductivity from Carbon Fiber Fillers Vertically Aligned by Electrostatic Flocking. *Adv. Mater.* **2014**, *26*, 5857−5862.
(52) Chen, H.; Ginzburg, V. V.; Yang, J.; Yang, Y.; Liu, W.; Huang, Y.; Du, L.; Chen, B. Thermal Conductivity of Polymer-Based Composites: Fundamentals and applications. *Prog. Polym. Sci.* **2016**, *59*, 41−85.
(53) Burger, N.; Laachachi, A.; Ferriol, M.; Lutz, M.; Toniazzo, V.; Ruch, D. Review of Thermal Conductivity in Composites: Mechanisms, Parameters and Theory. *Prog. Polym. Sci.* **2016**, *61*, 1−28.
(54) McGeary, R. K. Mechanical Packing of Spherical Particles. *J. Am. Ceram. Soc.* **1961**, *44*, 513−522.
(55) Sudduth, R. D. A New Method to Predict the Maximum Packing Fraction and the Viscosity of Solutions with a Size Distribution of Suspended Particles. II. *J. Appl. Polym. Sci.* **1993**, *48*, 37−55.
(56) Mostafaei, A.; Elliott, A. M.; Barnes, J. E.; Li, F.; Tan, W.; Cramer, C. L.; Nandwana, P.; Chmielus, M. Binder Jet 3D Printing—Process Parameters, Materials, Properties, Modeling, and Challenges. *Prog. Mater. Sci.* **2021**, *119*, No. 100707.
(57) Qi, R.; Li, N.; Du, J.; Shi, R.; Huang, Y.; Yang, X.; Liu, L.; Xu, Z.; Dai, Q.; Yu, D.; Gao, P. Four-dimensional vibrational spectroscopy for nanoscale mapping of phonon dispersion in BN nanotubes. *Nat. Commun.* **2021**, *12*, 1179.

https://doi.org/10.1021/acsnano.4c09346
ACS Nano XXXX, XXX, XXX−XXX

(58) Li, N.; Guo, X.; Yang, X.; Qi, R.; Qiao, T.; Li, Y.; Shi, R.; Li, Y.; Liu, K.; Xu, Z.; Liu, L.; García, Javier; de Abajo, F.; Dai, Q.; Wang, E.-G.; Gao, P. Direct observation of highly confined phonon polaritons in suspended monolayer hexgonal boron nitride. *Nat. Mater.* **2021**, *20*, 43−48.
(59) Guo, H.; Yan, W.; Sun, J.; Pan, Y.; He, H.; Zhang, Y.; Yang, F.; Wang, Y.; Zhang, C.; Li, R.; Liu, L.; Bai, S.; Wang, W.; Ye, Y.; Liu, T.-H.; Shiomi, J.; Zhang, X.; Song, B. Four-phonon scattering and thermal transport in 2H-$MoTe_2$. *Mater. Today Phys.* **2024**, *40*, No. 101314.
(60) Li, N.; Shi, R.; Li, Y.; Qi, R.; Liu, F.; Zhang, X.; Liu, Z.; Li, Y.; Guo, X.; Liu, K.; Jiang, Y.; Li, X.-Z.; Chen, J.; Liu, L.; Wang, E.-G.; Gao, P. Phonon transition across an isotopic interface. *Nat. Commun.* **2023**, *14*, 2382.
(61) Li, Y.; Zhang, X.; Wang, J.; Ma, X.; Shi, J.; Guo, X.; Zuo, Y.; Li, R.; Hong, H.; Li, N.; Xu, K.; Huang, X.; Tian, H.; Yang, Y.; Yao, Z.; Liao, P.; Li, X.; Guo, J.; Huang, Y.; Gao, P.; Wang, L.; Yang, X.; Dai, Q.; Wang, E.; Liu, K.; Zhou, W.; Yu, X.; Liang, L.; Jiang, Y.; Li, X.-Z.; Liu, L. Engineering Interlayer Electron−Phonon Coupling in WS_2/BN Heterostructures. *Nano Lett.* **2022**, *22*, 2725−2733.

https://doi.org/10.1021/acsnano.4c09346
ACS Nano XXXX, XXX, XXX−XXX